PCCP

PAPER

View Article Online
View Journal | View Issue

Cite this: *Phys. Chem. Chem. Phys.*, 2014, **16**, 4679

Chemical and morphological changes during olivine carbonation for CO_2 storage in the presence of NaCl and $NaHCO_3$

Greeshma Gadikota,[a] Juerg Matter,[bc] Peter Kelemen[b] and Ah-hyung Alissa Park*[ad]

Received 23rd November 2013,
Accepted 9th December 2013

DOI: 10.1039/c3cp54903h

www.rsc.org/pccp

The increasing concentrations of CO_2 in the atmosphere are attributed to the rising consumption of fossil fuels for energy generation around the world. One of the most stable and environmentally benign methods of reducing atmospheric CO_2 is by storing it as thermodynamically stable carbonate minerals. Olivine ($(Mg,Fe)_2SiO_4$) is an abundant mineral that reacts with CO_2 to form Mg-carbonate. The carbonation of olivine can be enhanced by injecting solutions containing CO_2 at high partial pressure into olivine-rich formations at high temperatures, or by performing *ex situ* mineral carbonation in a reactor system with temperature and pressure control. In this study, the effects of $NaHCO_3$ and NaCl, whose roles in enhanced mineral carbonation have been debated, were investigated in detail along with the effects of temperature, CO_2 partial pressure and reaction time for determining the extent of olivine carbonation and its associated chemical and morphological changes. At high temperature and high CO_2 pressure conditions, more than 70% olivine carbonation was achieved in 3 hours in the presence of 0.64 M $NaHCO_3$. In contrast, NaCl did not significantly affect olivine carbonation. As olivine was dissolved and carbonated, its pore volume, surface area and particle size were significantly changed and these changes influenced subsequent reactivity of olivine. Thus, for both long-term simulation of olivine carbonation in geologic formations and the *ex situ* reactor design, the morphological changes of olivine during its reaction with CO_2 should be carefully considered in order to accurately estimate the CO_2 storage capacity and understand the mechanisms for CO_2 trapping by olivine.

1. Introduction

The rising concentration of CO_2 in the atmosphere has detrimental environmental impacts and can be attributed to the increasing consumption of fossil fuels around the world. Therefore, various technologies and approaches for Carbon Capture, Utilization and Storage (CCUS), have been proposed to ensure more efficient carbon management. Among the carbon storage technologies, one of the safest and most permanent methods is carbon mineralization (also known as mineral carbonation), which mimics the natural process of mineral weathering. In experiments on abundant, rock forming minerals, other than the comparatively rare mineral, wollastonite, the mineral olivine ($(Mg,Fe)_2SiO_4$) has been found to have the most rapid carbonation rates.[1–3] Olivine is very far from equilibrium with the atmosphere and surface waters based on the Gibbs free energy quantified in Kelemen and Hirth.[4] Olivine is also known as the gemstone, peridot, and rocks with more than 40% olivine are called "peridotite". The Earth's upper mantle – from the base of the crust to a depth of ~400 km – is composed mainly of peridotite, with Mg/(Mg + Fe) ~ 0.9. Uplift and erosion exposes mantle peridotite on the surface during plate tectonic collisions. There are large deposits of olivine, including about 15 000 km^3 of peridotite in Oman in a block of oceanic crust and upper mantle thrust onto the Arabian continental margin (the Samail Ophiolite), which can be used for either *in situ* or *ex situ* carbon mineralization schemes.[1–5]

The carbon mineralization process involves the reaction of CO_2 with silicate minerals containing Mg and/or Ca.[6] As CO_2 is chemically fixed into the mineral matrix, it forms calcium and/or magnesium carbonates that are insoluble in water, thermally stable and environmentally benign.[7] Carbon mineralization is a multi-step process which involves CO_2 hydration as represented by reactions (1) – (3) followed by mineral dissolution (reaction (4)) and carbonation (reaction (5)) with the olivine Mg end-member,

[a] *Department of Chemical Engineering, Columbia University in the City of New York, New York, NY 10027, USA*
[b] *Lamont-Doherty Earth Observatory of Columbia University, Palisades, NY 10964, USA*
[c] *Department of Ocean and Earth Science, University of Southampton, Southampton, UK SO14 3ZH*
[d] *Department of Earth and Environmental Engineering, Columbia University in the City of New York, NY 10027, USA. E-mail: ap2622@columbia.edu; Fax: +1 212-854-7081; Tel: +1 212 854 8989*

forsterite (Mg_2SiO_4), as the representative mineral. Reaction (6) represents the overall reaction in which forsterite (Mg_2SiO_4) directly reacts with CO_2 in the aqueous phase to form magnesium carbonate minerals (here represented as magnesite, $MgCO_3$) + dissolved SiO_2 or solid SiO_2 phases (quartz, chalcedony or opal). Depending on reaction conditions such as temperature, CO_2 partial pressure, the presence of dissolved catalysts, pH, various reaction steps such as the extent of CO_2 hydration, the rate of mineral dissolution, and/or the rate of solid carbonate mineral nucleation and growth can have significant control over the rate of carbon mineralization. Many studies have discussed the kinetics of each step of CO_2 hydration,[8,9] forsterite dissolution,[10–17] and conditions that favor the formation of various Mg-carbonate phases.[18–20] Understanding the limiting factors when all three steps occur simultaneously requires further investigation since this has implications for *in situ* and *ex situ* carbon mineralization.

$$CO_2 \text{ hydration: } 2CO_{2(g)} \rightarrow 2CO_{2(aq)} \quad \text{(Rx. 1)}$$

$$2CO_{2(aq)} + 2H_2O \leftrightarrow 2H_2CO_{3(aq)} \leftrightarrow 2H_{(aq)}^{+} + 2HCO_{3(aq)}^{-} \quad \text{(Rx. 2)}$$

$$2HCO_{3(aq)}^{-} \leftrightarrow 2CO_{3(aq)}^{2-} + 2H_{(aq)}^{+} \quad \text{(Rx. 3)}$$

$$\text{Forsterite dissolution: } Mg_2SiO_{4(s)} + 4H_{(aq)}^{+} \rightarrow 2Mg_{(aq)}^{2+} + H_4SiO_{4(aq)} \quad \text{(Rx. 4)}$$

$$\text{Carbonate formation: } 2Mg_{(aq)}^{2+} + 2CO_{3(aq)}^{-} \rightarrow 2MgCO_{3(s)} \quad \text{(Rx. 5)}$$

$$\text{Overall reaction: } Mg_2SiO_{4(s)} + 2CO_{2(g)} + 2H_2O \rightarrow 2MgCO_{3(s)} + H_4SiO_{4(aq)} \quad \text{(Rx. 6)}$$

CO_2 can be directly injected into peridotite, or other silicate rocks with abundant Mg and Ca such as basalt,[1,2,21,22] to form solid carbonate minerals. This is known as *in situ* carbon storage. Another approach, referred to as *ex situ* carbon mineralization, involves mining and processing of silicate minerals prior to their reaction with CO_2.[23–28] For both *in situ* and *ex situ* carbon mineralization, a fundamental understanding of mineral dissolution and carbonation kinetics and the reaction mechanisms is important. A number of groups have carried out extensive work in this area.[1–4,7,10–29]

Much significant work has been carried out to investigate the effects of the reaction temperature and the CO_2 partial pressure on carbon mineralization. Mineral dissolution kinetics can be enhanced by increasing reaction temperatures,[10–14] which implies that the geothermal gradient can be utilized to enhance *in situ* carbon mineralization. Carbon mineralization is also found to be affected by the CO_2 partial pressure (P_{CO_2}) and at P_{CO_2} greater than 75 atm, the mineral carbonation process can be enhanced due to higher concentrations of carbonate species in the aqueous phase.[26,27] Moreover, the reaction temperature and P_{CO_2} values affect the chemical compositions of the formed magnesium carbonates.[18–20] At higher temperatures, anhydrous magnesium carbonate is formed (*i.e.*, magnesite, $MgCO_3$), while at lower temperatures hydrated magnesium carbonates such as nesquehonite ($MgCO_3 \cdot 3H_2O$) and hydromagnesite ($Mg_5(CO_3)_4(OH)_2 \cdot 4H_2O$) are dominant in experimental studies.

In important studies that guided our choices of reagents, O'Connor *et al.*,[27] at the Department of Energy's Albany Research Center (ARC) and Chizmeshya *et al.*,[28] at Arizona State University investigated olivine carbonation in CO_2 saturated aqueous solutions at varying temperature and P_{CO_2}, with the important addition of dissolved NaCl and bicarbonate compounds (mostly $NaHCO_3$, but also $KHCO_3$ and $RbHCO_3$). These groups found that the presence of these reagents, typically 1.0 M NaCl and 0.64 M $NaHCO_3$, led to a substantial enhancement in the olivine reaction rate, when compared to studies of olivine dissolution at the same temperature, P_{CO_2} and pH.[2,3] However, the "separation of variables" was not completed, so that the independent, potentially catalytic roles of NaCl and $NaHCO_3$ were not well established.

Another important but less studied aspect of the carbon mineralization study is related to the changes in the structural features of the minerals such as the pore volume, surface area and particle size during the dissolution and carbonation processes of silicate minerals. Some studies have suggested that extensive carbonate growth may exert high crystallization pressures sufficient to create microfractures in geologic formations which would expose additional unreacted mineral surface and increase the CO_2 storage capacity.[1,4] Others argue that the formation of carbonate crystals in minerals would simply block the pore spaces, reduce the reactive surface area and significantly slow down the *in situ* carbon mineralization process.[29,30]

This study investigated a number of these questions regarding reaction kinetics and mechanisms during carbon mineralization. The carbonation of one of the most widely investigated minerals, olivine, was studied to understand the corresponding changes in the chemical compositions and morphological structures during CO_2–olivine–water interactions. In addition to determining the morphological changes, there has been a considerable debate and an emerging concern related to appropriate methods for the quantification of CO_2.[31] Therefore, the extents of carbonation were estimated using two separate methods: Thermogravimetric Analysis (TGA) and Total Carbon Analysis (TCA).

2. Experimental methods

Ground Twin Sisters olivine procured from Washington State was provided by the group at Albany Research Center (ARC). Table 1 summarizes the composition of olivine. The mean particle size, surface area and cumulative pore volume of the

Table 1 Composition of Twin Sisters olivine

Components	Weight%	Components	Weight%
MgO	47.30	MnO	0.15
CaO	0.16	Na_2O	0.01
Fe_2O_3	13.90	K_2O	<0.01
SiO_2	39.70	TiO_2	<0.01
Cr_2O_3	0.78	P_2O_5	<0.01
Al_2O_3	0.20	V_2O_5	<0.01
		LOI%	−0.7

ground unreacted olivine sample were found to be 21.40 μm, 3.77 $m^2 g^{-1}$ and 0.012 ml g^{-1}, respectively.

2.1. Carbonation of olivine

The carbonation experiments were performed in a high temperature, high pressure batch reactor (Autoclave Engineers, 100 ml EZE-Seal) and the schematic of the experimental setup is shown in Fig. 1. The reactor was connected to a high-pressure syringe pump (Teledyne Isco, 500D, NE), which can deliver up to 200 atm of pressurized CO_2 to the reactor. In a typical run, 50 ml of slurry containing 15 wt% of solids in the reaction fluid was charged into the reactor. The reactor was then sealed and the stirring speed was set at 800 rpm throughout the experiment since it was the optimum speed for effective mass and heat transfer within the reactor. Once the reactor temperature set-point was specified, it took about 30 minutes for the reactor temperature to be stabilized. After the desired reaction temperature was reached, the reactor pressure was increased to the desired partial pressure of CO_2, which marked the start of the experiment. These experiments were performed with an ultra-high purity grade of CO_2 (99.99%) to mimic a pure and pressurized stream of CO_2 that would be obtained from various CO_2 capture processes. It generally took about 75 minutes to cool the reactor to below 70 °C. At the end of the specified reaction time (*i.e.*, 1–5 hours) and cooling period, liquid and solid samples were collected. The interior of the reactor was rinsed in water, and this water was filtered to obtain any solid material that had formed on the vessel walls. The filtered liquid samples were diluted ten times into 2% HNO_3 solution to prevent any subsequent precipitation, while the carbonated solid samples were dried at 70 °C for 12 hours. The amounts of dissolved Mg and other components (*i.e.*, Si), which did not form solid phases, were quantified *via* elemental analysis of the liquid samples using Inductively Coupled Plasma-Atomic Emission Spectroscopy (ICP-AES, Activa S model, Horiba Jobin Yvon).

2.2. Quantification of mineralized CO_2

Both unreacted mineral and carbonated solid products were dried and analyzed using a battery of experimental techniques.

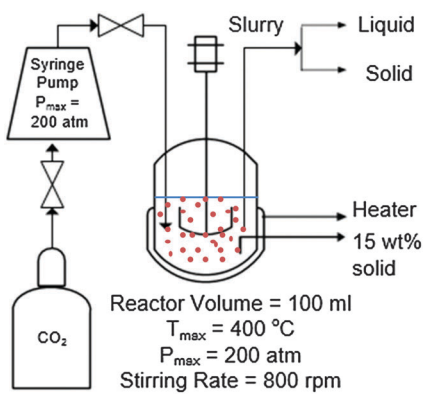

Fig. 1 Schematic of high pressure, high temperature experimental setup for mineral carbonation.

The elemental compositions of the solid samples were determined using Wavelength Dispersion X-ray Fluorescence (WD-XRF, Panalytical Axios). The X-ray diffraction patterns were also obtained (XRD 3000, Inel Inc.) in the range of 20° and 80° and CuKα radiation (λ = 1.5406 Å) to identify the changes in chemical compositions and crystalline structures during the carbonation reaction. The extent of carbonation was determined using two separate methods: Thermogravimetric Analysis (TGA, Setaram SETSYS) and Total Carbon Analysis (TCA, LECO CS 844).

In a typical TGA run, samples were exposed to a N_2 environment (flow rate: 20 ml min^{-1}) as the temperature was ramped from 25 °C to 650 °C at a rate of 5 °C min^{-1}.[32] Based on the weight drop related to each dehydroxylation or calcination temperature, the carbonate phase in the solid sample was identified and the extent of carbonation was determined based on the weight drop data (wt% in terms of [g of gas released/g of carbonated solids]). The estimation of the extent of carbonation based on the TGA method provided an insight into the presence of different solid phases (*e.g.*, carbonate and hydrate phases as well as organic carbon with distinct decomposition temperature) and the quantification of each phase in the analyzed sample. On the other hand, the TGA technique can be difficult for samples with overlapping weight drop curves. Thus, the TGA method should be used for samples with clear distinction between weight drop curves, and this was the case for carbonated olivine samples.

In a typical TCA run, samples were placed in a ceramic boat and combusted in the presence of O_2 at temperatures as high as 1000 °C. The combustion process converts all carbon – both inorganic and organic – into CO_2 and CO. The total carbon reported from the TCA [g of C/g of carbonated solids] was then converted into the extent of carbonation by comparing the TCA data with the theoretical carbon capture capacity of the minerals. The TCA generally provides much faster measurements compared to TGA and is relatively more accurate in measuring the total carbon content in solid samples. However, it cannot distinguish different carbonate or hydrate phases as well as organic carbon in solid samples. Thus, the carbon analysis unit should be used in a Total Inorganic Carbon (TIC) mode using acid digestion, especially when organic additives such as oxalate are present in the reaction fluid. However, the acid digestion method is quite slow compared to the TCA method. Since the reaction fluids used in our study did not contain organic additives, the TCA mode was used in conjunction with the TGA technique to estimate the extents of carbonation for olivine, and the results of both methods were compared to assess consistency.

2.3. Characterization of morphological properties

The changes in the pore structure and the specific surface area were determined using the BET technique (Quantachrome NovaWin BET Analyzer), while particle size and size distributions were determined using a laser diffraction method (Beckman Coulter, Inc., LS 13 320 MW). The surface morphological features and the corresponding elemental concentrations

of mineral carbonates were determined using a Scanning Electron Microscope (SEM, Tescan Vega II) linked to an Energy Dispersive X-ray Spectrometer (EDS, Oxford Instruments, Inca Software).

3. Results and discussion

3.1. Estimation of extent of carbonation

The determination of the extent of mineral carbonation can be difficult, particularly if the minerals involved are highly heterogeneous. Even for a homogeneous mineral specimen, the preparation of samples (*e.g.*, different grinding methods resulting in distinct particle size distributions) can alter the carbonation results. Thus, the extent of mineral carbonation should be carefully estimated based on the mineralogy of the samples tested. In this study, the extent of carbonation was estimated relative to the theoretical carbon storage capacity of a mineral, $\frac{1}{R_{CO_2}}$, which is defined as the mass of CO_2 that can be trapped in a unit mass of the unreacted mineral. Conversely, R_{CO_2} refers to the amount of the mineral needed to store a unit mass of CO_2.[27]

The chemical fixation of CO_2 in the mineral matrix generally involves the leaching of alkaline metal ions into the aqueous phase and a subsequent carbonation reaction, represented by reaction (7).

$$M_{(aq)}^{n+} + \frac{n}{2}CO_{3(aq)}^{2-} \rightarrow M(CO_3)_{\frac{n}{2}(s)} \qquad (Rx.7)$$

where M is an alkaline metal such as Ca, Mg and Fe that can react with CO_2 to form insoluble and thermodynamically stable mineral carbonates. Therefore, the CO_2 storage capacity of minerals, $\frac{1}{R_{CO_2}}$, can be expressed as following.

$$\frac{W_{CO_2}}{W_{mineral}} = \frac{1}{R_{CO_2}} = \sum\left(\frac{n}{2}\cdot\frac{y_m}{MW_m}\right) \times MW_{CO_2} \qquad (1)$$

where W_{CO_2} and $W_{mineral}$ are weights of CO_2 stored in the solid phase and the mineral before its carbonation, respectively. y_m refers to the mass fraction of alkaline metal in the mineral that can react with CO_2 to form insoluble metal carbonate. MW_m is the molecular weight of alkaline metal species and $\frac{n}{2}$ refers to the stoichiometric coefficient of CO_2 as represented in reaction (7). The divalent alkaline metal species, Mg, Ca and Fe, are the most abundant alkaline metals that form carbonate minerals, with $\frac{n}{2} = 1$, and thus, eqn (1) can be simplified to eqn (2) below.

$$\frac{W_{CO_2}}{W_{mineral}} = \frac{1}{R_{CO_2}} = \left(\frac{y_{Mg}}{MW_{Mg}} + \frac{y_{Ca}}{MW_{Ca}} + \frac{y_{Fe}}{MW_{Fe}}\right) \times MW_{CO_2} \qquad (2)$$

While iron(II) oxide can react with CO_2 to form siderite ($FeCO_3$), it has been reported that the formation of siderite is inhibited by the low solubility of iron oxide, which may precipitate from the solution before siderite is formed.[27] Thus, in this paper the CO_2 storage capacity of olivine was calculated using both equations that were developed assuming the formation of iron carbonate (eqn (2)) and the absence of iron carbonate (eqn (3)).

$$\frac{W_{CO_2}}{W_{mineral}} = \frac{1}{R_{CO_2}} = \left(\frac{y_{Mg}}{MW_{Mg}} + \frac{y_{Ca}}{MW_{Ca}}\right) \times MW_{CO_2} \qquad (3)$$

The yield or the extent of carbonation, Y_{CO_2}, is then defined as the measured amount of CO_2 stored in the mineral as solid carbonate relative to the CO_2 storage capacity given by eqn (2) or (3). In this study, separate expressions of Y_{CO_2} have been developed for the two different carbon analysis techniques, eqn (4) and (5). Where the TGA method was used to analyze the carbonated solids, the following expression was used to determine the yield or extent of carbonation, $Y_{CO_2,TGA}$.

$$Y_{CO_2,TGA} = \left[\frac{\text{Measured weight ratio of } CO_2 \text{ stored in mineral}}{\text{The residual } CO_2 \text{ storage capacity}}\right] \times 100\%$$
$$= \frac{\left(\frac{W_{CO_2}}{W_{mineral}}\right)}{\left(\frac{1}{R_{CO_2}}\right)} \times 100\% = R_{CO_2} \times \left(\frac{TGA}{(100 - TGA)}\right) \times 100\% \qquad (4)$$

where TGA represents the percent weight change of the carbonated solid at its calcination temperature. On the other hand, eqn (5) was used when TCA was used for the solid analysis.

$$Y_{CO_2,TCA} = R_{CO_2} \times \left(\frac{3.67 \times TCA}{(1 - 3.67 \times TCA)}\right) \times 100\% \qquad (5)$$

where TCA represents the weight fraction of carbon in the carbonated sample with a unit of $\left[\frac{\text{Weight of carbon}}{\text{Weight of solid sample}}\right]$. The coefficient 3.67 is introduced into eqn (5) to account for the ratio of the molecular weights of CO_2 to carbon. The extents of carbonation using TGA and TCA are compared in Fig. 3(a), 4(a), 7(a) and 8(a). The averages of TGA and TCA estimates are represented in Table 2.

3.2. Effect of reaction time

Investigation of the effect of the reaction time on the extent of olivine carbonation provided insight into the kinetics of mineral carbonation. Changes in the morphological structure of olivine as a function of the reaction time were also probed to study reaction mechanisms. Experiments were performed at reaction times of 1, 3 and 5 hours, at 185 °C, and P_{CO_2} of 139 atm (P_{total} = 150 atm) in 1.0 M NaCl + 0.64 M $NaHCO_3$ with 15 wt% solid and a stirring rate of 800 rpm. These were the reaction conditions used in prior studies, including those conducted by the ARC group.[26,27] The extents of olivine carbonation were estimated using both TGA and TCA methods, and their average values are reported in Table 2 and Fig. 2(a). These results were compared with the results of similar studies at ARC.[26,27] Average values of olivine carbonation range from 49.4 to 79.1% assuming the formation of Ca, Mg, and Fe carbonates

Table 2 Summary of mean particle sizes, surface areas and extents of carbonation of olivine reacted at varying reaction times, temperatures, CO_2 partial pressures and chemical additives. The slurry concentration was 15 wt% and a stirring speed of 800 rpm was maintained. Extents of carbonation are reported as an average of TGA and TCA estimates

			Extent of carbonation (%)	
	Mean particle size (μm)	Surface area ($m^2\ g^{-1}$)	Assuming the formation of Ca, Mg and Fe carbonates	Assuming the formation of Ca and Mg carbonates
Effect of reaction time (185 °C, P_{CO_2} = 139 atm, 1.0 M NaCl + 0.64 M $NaHCO_3$)				
1 hour	23.97	1.25	49.4 ± 1.3	56.6 ± 1.5
3 hours	27.34	0.96	74.6 ± 2.6	85.3 ± 3.1
5 hours	27.70	0.15	79.1 ± 4.9	90.5 ± 5.6
Effect of partial pressure of CO_2 (185 °C, 3 hours, 1.0 M NaCl + 0.64 M $NaHCO_3$)				
64 atm	20.69	3.20	34.3 ± 0.8	39.3 ± 0.9
89 atm	26.19	1.73	52.3 ± 1.9	59.9 ± 2.1
139 atm	27.34	0.96	73.5 ± 2.8	85.3 ± 3.1
164 atm	27.96	0.80	73.3 ± 2.5	83.9 ± 2.8
Effect of temperature (P_{CO_2} = 139 atm, 3 hours, 1.0 M NaCl + 0.64 M $NaHCO_3$)				
90 °C	15.36	2.01	2.6 ± 0.3	3.0 ± 0.3
125 °C	18.51	1.10	24.6 ± 0.3	28.2 ± 0.4
150 °C	25.40	1.07	61.6 ± 1.6	70.5 ± 1.8
185 °C	27.34	0.96	73.5 ± 2.8	85.3 ± 3.1
Effect of [$NaHCO_3$] (185 °C, P_{CO_2} = 139 atm, 3 hours)				
Deionized water	16.43	2.79	5.0 ± 0.3	5.8 ± 0.3
0.32 M $NaHCO_3$	17.64	1.63	9.5 ± 0.7	10.9 ± 0.8
0.48 M $NaHCO_3$	26.54	1.51	49.0 ± 0.4	56.0 ± 0.5
0.64 M $NaHCO_3$	26.58	1.20	72.2 ± 3.1	82.7 ± 3.6
1.00 M $NaHCO_3$	29.43	1.15	74.3 ± 1.7	85.0 ± 1.9
2.00 M $NaHCO_3$	30.02	1.15	79.7 ± 5.2	91.2 ± 6.0
Effect of [NaCl] (185 °C, P_{CO_2} = 139 atm, 3 hours)				
Deionized water	16.43	2.79	5.0 ± 0.3	5.8 ± 0.3
0.50 M NaCl	14.87	2.54	5.9 ± 0.3	6.8 ± 0.3
0.75 M NaCl	17.06	2.50	9.0 ± 0.5	10.3 ± 0.6
1.00 M NaCl	17.16	2.50	12.8 ± 0.4	14.4 ± 0.9

and from 56.6 to 90.5% assuming Ca and Mg carbonate formation (Table 2, Fig. 2(a)). These results were compared with the results of similar studies at ARC.[26,27]

As discussed earlier, estimating the extent of olivine carbonation proved to be a challenge due to the role of iron. The potential formation of Fe-carbonates (*i.e.*, siderite) has been debated.[26,27,33] As a result of their low solubility, iron oxide minerals may precipitate prior to the formation of siderite. In this study, siderite was not detected in any XRD analysis of carbonated olivine samples. Both eqn (2) and (3) were used to estimate the extent of olivine carbonation in order to compare our results with those of the ARC group. As summarized in Table 2, the extents of olivine carbonation *via* formation of Ca- and Mg-carbonates were 56.6, 85.3 and 90.5% for 1, 3 and 5 hour reactions, respectively. These values are 7 to 11% higher than estimates made including the formation of siderite as well as Ca- and Mg-carbonates. The extent of olivine carbonation calculated for Fe-, Ca- and Mg carbonates resulted in values close to those of the ARC, since ARC included all of these in their calculations. In any case, the rate of olivine carbonation was reduced after 3 hours in our results and those of the ARC, as shown in Fig. 2(a).

The analysis of fluid samples revealed that the total concentration of the Mg-species was 39.8, 27.6 and 24.5 ppm at the end of 1, 3 and 5 hour reactions, respectively. These values are significantly lower than the equilibrium total Mg concentration of 218 ppm at the given reaction conditions based on PhreeqC[34] calculations. The concentration of Mg in solution could increase over time due to olivine dissolution alone, and decrease due to precipitation of carbonate minerals. In our experiments, combined olivine dissolution and carbonate precipitation resulted in a net decrease in the concentration of Mg in solution over time. This implies that as olivine dissolved to release Mg into solution, the dissolved species were readily carbonated to precipitate magnesium carbonates. This indicates that olivine dissolution may have been the rate limiting step in the process. Also, because precipitation of Mg-carbonates held dissolved Mg concentrations below the equilibrium level, olivine dissolution rates may have remained relatively high throughout the experiments.

In order to provide further insights into the olivine carbonation mechanism, the changes in the morphological structure of olivine in terms of the surface area, particle size and pore volume distributions were investigated. As olivine was carbonated for 1, 3 and 5 hours, its mean particle size increased from 21.40 μm to 23.97, 27.34 and 27.70 μm, respectively (Table 2). A comparison of the particle size distributions before and after carbonation revealed that fine particles smaller than 10 μm dissolved much faster than coarser grains, resulting in a narrower particle size distribution shifted towards larger particle

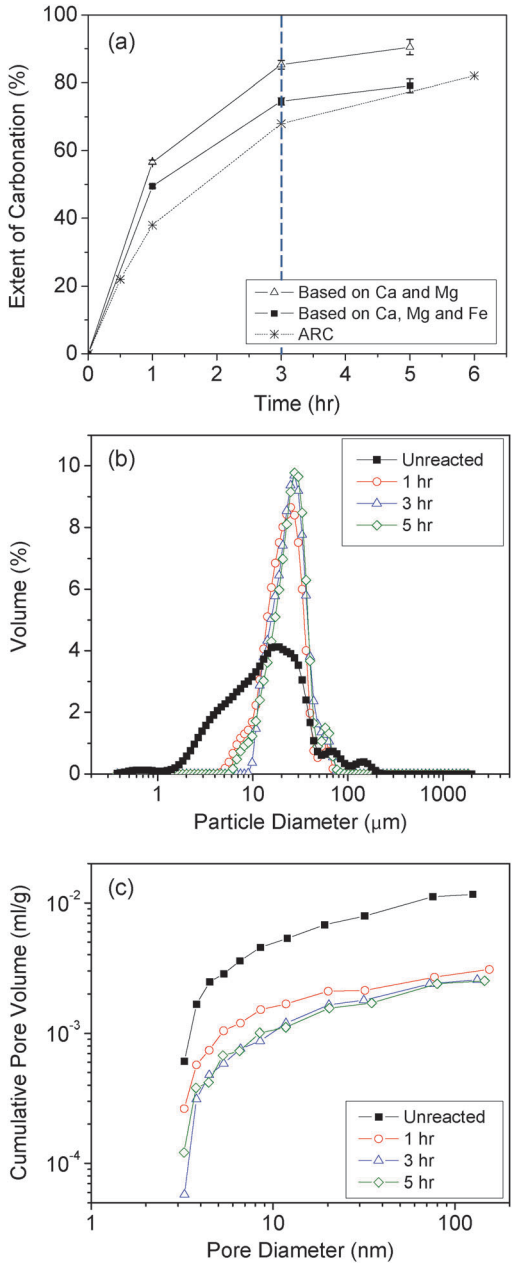

Fig. 2 Effect of reaction time on (a) extent of olivine carbonation based on two CO_2 storage capacity calculations (eqn (2) and (3)), (b) particle size distribution, and (c) cumulative pore volume. Experiments were conducted at 185 °C, P_{CO_2} = 139 atm in 1.0 M NaCl + 0.64 M $NaHCO_3$ with 15 wt% solid and a stirring speed of 800 rpm. The ARC study was performed under same conditions but for 1 hour, P_{CO_2} = 150 atm, 1000 rpm, and included Fe-carbonate formation.[27]

sizes (Fig. 2(b)). Precipitation of carbonates on olivine surfaces also contributed to increasing particle size. The particle size distributions of 3 and 5 hour runs were not significantly different, as they had similar extents of carbonation. BET analyses also showed a significant reduction in surface area, from an initial value of 3.77 to 1.25, 0.96 and 0.15 $m^2\ g^{-1}$ when olivine was reacted for 1, 3 and 5 hours, respectively. A similar trend was observed for the cumulative pore volume of olivine during the experiments. A reduction in the cumulative pore volumes from 0.0120 to 0.0030, 0.0026 and 0.0025 ml g^{-1} was observed when olivine was reacted for 1, 3 and 5 hours, respectively (Fig. 2(c)). The reduction of the surface area and the pore volume suggest the rapid disappearance of fine particles with high surface to volume ratios (<10 μm) as well as the growth of carbonate precipitates in the pores and surfaces of olivine particles.

These morphological data are valuable since mineral weathering studies typically assume negligible changes in the surface area and the pore volume during reactions, which is not always the case. Therefore, throughout this study the discussion of the extent of olivine carbonation is accompanied by its morphological change results.

3.3. Effect of partial pressure of CO_2

Since pressures of 100–150 atm have been considered as the optimum pressure for CO_2 transportation in pipelines, most previous studies on mineral carbonation were performed within this P_{CO_2} range.[26,27] In order to more fully quantify the effect of CO_2 pressure on mineral carbonation rates, our experiments were performed at P_{CO_2} values ranging from 64 to 164 atm, while holding other reaction parameters constant at 185 °C in 1.0 M NaCl + 0.64 M $NaHCO_3$ (as in many previous experiments at ARC and Arizona State University[26–28]) for 3 hours with 15 wt% solid and at a stirring rate of 800 rpm. The extent of olivine carbonation at 64, 89, 139 and 164 atm was 39.3, 59.9, 85.3 and 83.9%, respectively, based on the average value of TCA and TGA data assuming the formation of Ca and Mg-carbonates.

As shown in Fig. 3(a), the difference between TCA and TGA data were not significant. The complete list of carbonation data is given in Table 2, where the extents of olivine carbonation are reported as an average of TGA and TCA estimates for both eqn (2) and (3). The extents of carbonation were lower by about 5% and 10% for cases with low and high extents of carbonation, respectively, if the potential formation of siderite was included. In any case, a significant increase in the extent of carbonation from 64 atm to 139 atm was observed, while the extents of carbonation leveled off beyond 139 atm. The ARC group's 1 hour experiments agreed with this observation.[26,27]

Ignoring the result for the experiment at 164 atm, because olivine was almost completely consumed at both 139 and 164 atm, the net rate of olivine carbonation (mass fraction per second) could be represented by the following equation where P_{CO_2} is in atm.

$$\text{Rate of olivine carbonation} = -5.13 \times 10^{-5} + 1.11 \times 10^{-5}\sqrt{P_{CO_2}} \quad (6)$$

Strikingly, despite differences in grain size and experimental run duration, the dependence on P_{CO_2} in this study was almost identical to the slope of the expression fit to the results of O'Connor *et al.*[27] by Kelemen and Matter[1] as represented by the following equation.

$$\text{Rate of olivine carbonation} = 1.15 \times 10^{-5}\sqrt{P_{CO_2}} \quad (7)$$

The rate of reaction in our study was systematically ~2× slower than the extent of reaction in the ARC study at a similar

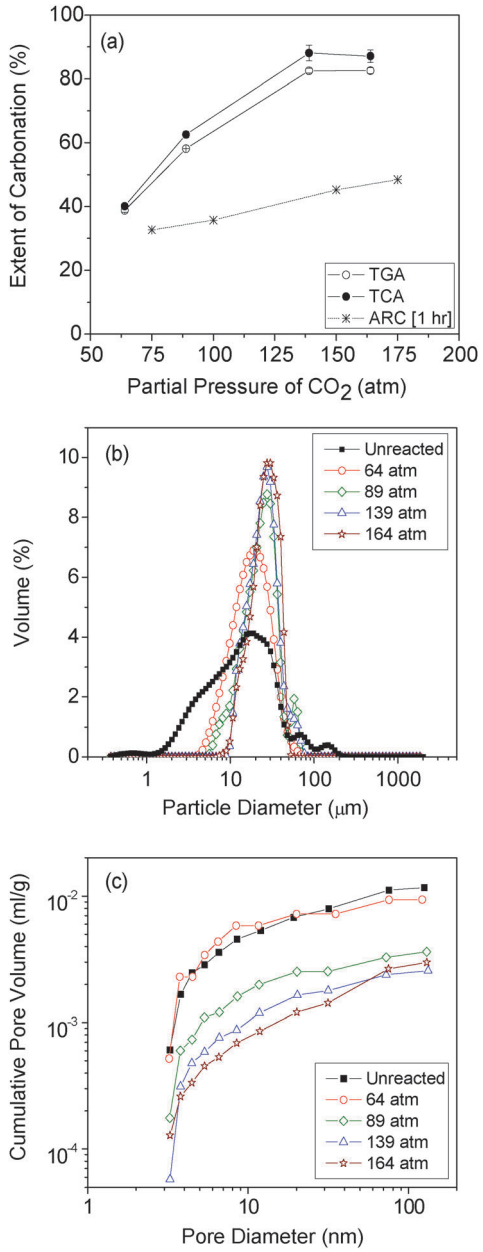

Fig. 3 Effect of CO_2 partial pressure on (a) extent of olivine carbonation based on the formation of Mg and Ca carbonates, (b) particle size distribution, and (c) cumulative pore volume. Experiments were conducted at 185 °C in 1.0 M NaCl + 0.64 M $NaHCO_3$ for 3 hours, with 15 wt% solid and a stirring speed of 800 rpm. ARC study was performed under same conditions but 1 hour, P_{CO_2} = 150 atm, 1000 rpm, and included Fe-carbonate formation.[27]

temperature and P_{CO_2} (see Kelemen and Matter 2008, Supplementary Figures S5 and S4).[1] A combined fit for the two datasets resulted in the following expression that is quite similar to the expression for each dataset individually.

$$\text{Rate of olivine carbonation} = 1.031 \times 10^{-5}\sqrt{P_{CO_2}} \qquad (8)$$

The CO_2 pressure influences a number of parameters during aqueous mineral carbonation including the pH of the solution, the dissolution of carbon into the aqueous phase, and speciation of dissolved carbon in bicarbonate and carbonate ions. In order to investigate the effect of P_{CO_2} on these parameters, PhreeqC modeling was performed for a closed system of forsterite-reaction fluid-CO_2. Forsterite, Mg_2SiO_4 (no Ca or Fe), is the Mg-end member of the olivine solid solution series, and is included in the PhreeqC database. As expected, the equilibrium pH of the solution, calculated using PhreeqC, decreased from 6.65 to 6.53, 6.36 and 6.29 as the partial pressure of CO_2 was increased from 64 atm to 89, 139 and 164 atm, respectively. While this change in the pH is relatively small, the mineral carbonation is a multistep process with a number of parallel and competing reactions. At low pH, olivine dissolution is rapid, but precipitation of $MgCO_3$ is limited. At high pH, $MgCO_3$ forms readily, but olivine dissolution is very slow. Our experiments and previous work revealed that high concentrations of $NaHCO_3$ in solution buffer pH at intermediate values where both olivine dissolution and carbonate precipitation are both favored. The high CO_2 pressure caused higher solubility of carbon species in the fluid, increasingly high compared to equilibrium values for $MgCO_3$ precipitation. A detailed investigation of the role of CO_2 hydration in olivine carbonation is given in Section 3.5.

Particle size analyses of carbonated solids showed that the mean particle size did not change significantly when olivine was carbonated at 64 atm, whereas at 89, 139 and 164 atm, the particle size increased from 21.40 to 26.19, 27.34 and 27.96 μm, respectively (Table 2). The particle size distributions provide more insights into the olivine carbonation mechanism. In all cases, the number of fines decreased significantly and progressively, and the particle size distributions became narrower and shifted towards larger sizes with increasing P_{CO_2} (Fig. 3(b)). The extents of olivine carbonation for the 139 and 164 atm cases were quite similar at about 84–85%, and the particle size distribution results matched as well (Fig. 3(a) and (b) and Table 2).

The increase in particle size is also reflected in the changing surface area and pore volume of carbonated olivine. The surface area of the olivine decreased from 3.77 $m^2\ g^{-1}$ for unreacted olivine to 3.20, 1.73, 0.96 and 0.80 $m^2\ g^{-1}$ at 64, 89, 139 and 164 atm, respectively (Table 2). The cumulative pore volume followed the same trend as surface area. The cumulative pore volume decreased from 0.012 ml g^{-1} for unreacted olivine to 0.0094, 0.0036, 0.0026 and 0.0029 ml g^{-1} for samples carbonated at 64, 89, 139 and 164 atm, respectively (Fig. 3(c)). The observed simultaneous changes in composition and morphology suggest that conventional methods of estimating mineral dissolution and carbonation rates assuming constant pore volume and surface area during mineral carbonation may have resulted in significant inaccuracy in rate estimation.

3.4. Effect of reaction temperature

A number of studies have investigated the effect of temperature on olivine dissolution[10–14] and carbonation.[26–28] Previous results indicate that dissolution is favored at high temperature, while olivine carbonation rate is maximized at ~185 °C over a range of P_{CO_2}. Furthermore, it was also reported that magnesite, $MgCO_3$ – rather than hydrated magnesium carbonate minerals such as nesquehonite and hydromagnesite – forms at higher

reaction temperatures, as we found in this study. In all of our experiments (90–185 °C), the precipitated Mg-carbonate phase was magnesite. While the chemical compositions of the carbonated species have been well documented for various reaction conditions, the corresponding morphological features have not been well understood. Thus, a series of olivine carbonation experiments were performed while monitoring the particle size, the surface area, and particle size and pore volume distributions. The temperature range of 90 to 185 °C was selected since it is the temperature range commonly present at CO_2 injection sites. The experiments were performed in a solution of 1.0 M NaCl + 0.64 M $NaHCO_3$ at P_{CO_2} = 139 atm for 3 hours with 15 wt% solid and at a stirring rate of 800 rpm.

The extents of olivine carbonation at 90, 125, 150 and 185 °C were found to be 3.0, 28.2, 70.5 and 85.3%, respectively considering the formation of Mg and Ca-carbonates. These are the average values of the TGA and TCA data, which were quite consistent (Fig. 4(a)). The ARC's results obtained for one hour olivine carbonation study were compared to this study as shown in Fig. 4(a) and the trend was very similar.[26,27]

These experimental results were well fit by the following expression (eqn (9)) which was strikingly identical to the fit (eqn (10)) obtained by Kelemen and Matter[1] for the experimental data of O'Connor *et al.*,[27] despite differences in fluid/rock ratio, grain size and run duration. In the following equations, the unit of temperature is Celsius.

$$\text{Rate of olivine carbonation} = 9.3 \times 10^{-5} + e^{\left(-0.000383 \times (T-185)^2\right)} \quad (9)$$

$$\text{Rate of olivine carbonation} = 1.38 \times 10^{-4} + e^{\left(-0.000334 \times (T-185)^2\right)} \quad (10)$$

The expressions were similar despite the fact that time series results, both in our study and the ARC results, showed decreasing carbonation rates with reaction times varying from 1 to 3 hours. This temporal decrease in rates was relatively unimportant because the combined effects of temperature and P_{CO_2}, in the presence of $NaHCO_3$-rich aqueous solutions, yielded a four to five orders of magnitude variation in the experimental extents of olivine carbonation at temperatures from ~25 to 250 °C and P_{CO_2} from ~20 to 250 atm in the ARC results, and a one to two orders of magnitude variation in our new results (90–185 °C, P_{CO_2} of 64 to 164 atm). A combined fit for our new data and those of O'Connor *et al.*[27] yielded the following expression:

$$\text{Rate of olivine carbonation} = 1.13 \times 10^{-4} + e^{\left(-0.000330 \times (T-185)^2\right)} \quad (11)$$

The consistency between these studies, and our other results described below, suggested that the rate expressions derived by Kelemen and Matter[1] can be confidently used for order-of-magnitude estimation of olivine carbonation rates as a function of temperature and P_{CO_2} in aqueous fluids with >0.5 M $NaHCO_3$ with olivine grain sizes of tens of microns.

A more comprehensive expression of the olivine carbonation rate incorporating temperature and partial pressure of CO_2 using

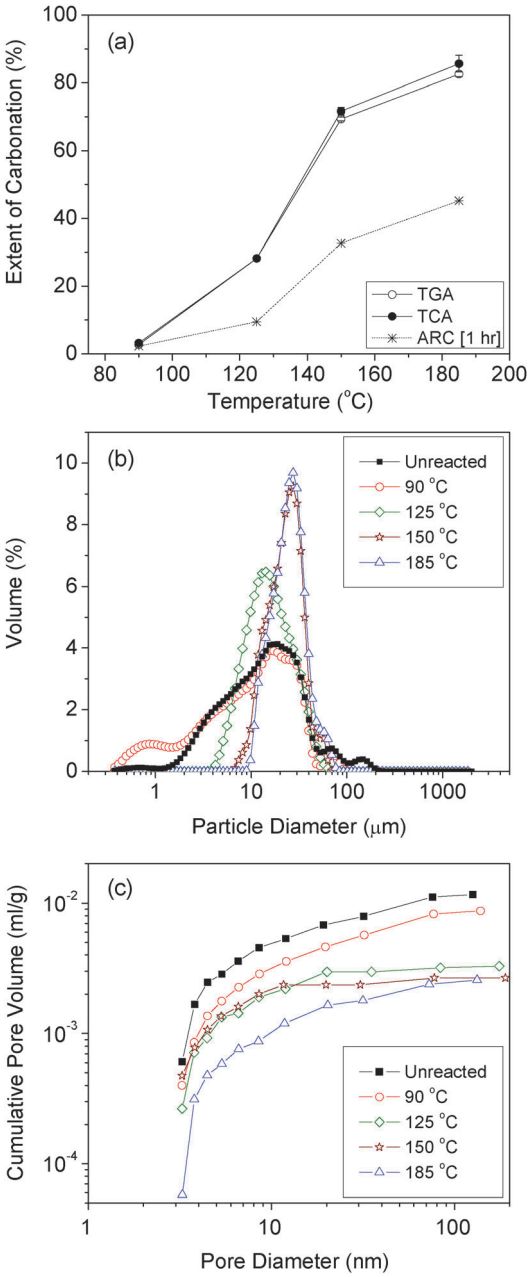

Fig. 4 Effect of temperature on (a) extent of olivine carbonation based on the formation of Mg and Ca carbonates, (b) particle size distribution, and (c) cumulative pore volume. Experiments were conducted at P_{CO_2} = 139 atm in 1.0 M NaCl + 0.64 M $NaHCO_3$ for 3 hours, with 15 wt% solid and a stirring speed of 800 rpm. ARC study was performed under same conditions but 1 hour, P_{CO_2} = 150 atm, 1000 rpm, and included Fe-carbonate formation.[27]

ARC results[27] in the presence of aqueous fluids with more than ~0.5 M $NaHCO_3$, with grain sizes of tens of microns was developed by Kelemen and Matter[1] as represented by eqn (12).

$$\text{Rate of olivine carbonation} = 1.15 \times 10^{-5} \sqrt{P_{CO_2}} \times e^{-0.00033 \times (T-185)^2} \quad (12)$$

A modified expression fit to our new results as well as the ARC results[27] which was very similar to eqn (12) is also

represented below.

$$\text{Rate of olivine carbonation} = 1.03 \times 10^{-5}\sqrt{P_{CO_2}} \times e^{-0.00033\times(T-185)^2} \quad (13)$$

The small differences in the rate expressions are attributed to the uncertainty in olivine carbonation rates under the relevant experimental conditions.

Small deviations between our new data and the results of the ARC study were mainly due to the longer reaction times in our experiments, and the fact that we did not include carbonation of Fe for the Y_{CO_2} calculations in this study, as discussed in a previous section. The differences in the extents of carbonation when siderite formation was included *vs.* not considered were 0.4% at 90 °C and 10% at 185 °C, as shown in Table 2. Solution analyses revealed the relative rates of mineral dissolution and carbonation at different temperatures. Mg concentrations in the fluid samples collected at the end of each run were 106.0, 87.3, 38.2 and 27.6 ppm at 90, 125, 150 and 185 °C, respectively. These concentrations were measured after the reactor was cooled, depressurized, and the slurry was filtered at ambient temperature. However, comparing these concentrations with equilibrium concentrations was challenging because simulations suggested that the speciation may have changed significantly as the reaction was quenched and the reactor was depressurized. Quenching effects on the solubility of various species vary with temperature, but were found to be negligible compared to the mass of magnesite precipitated in the higher temperature experiments.

The effect of the increase in reaction temperature on olivine carbonation could be complex. For instance, a higher temperature would (i) lower CO_2 solubility, (ii) in turn, increase the solution pH, (iii) favor mineral dissolution, (iv) enhance mineral dissolution and carbonation kinetics, and (v) reduce the solubility of magnesite.[35] To probe the temperature effect, a series of PhreeqC[34] thermodynamic simulations were performed using the Lawrence Livermore National Laboratory (LLNL) thermodynamic database. These simulations revealed that the solubility of magnesite decreases significantly with increasing temperature. In addition, the simulations revealed that the pH of the solution equilibrated with CO_2 were 6.19, 6.24 and 6.51 at 90, 125 and 185 °C, respectively. As temperature increased from 90 to 185 °C, the pH was increased by only 0.32. While past studies have indicated that small changes in pH have a minor effect on olivine dissolution,[36] it is important to note that pH changes can impact carbonate concentrations. An equivalent change in the pH of 0.32 increased the concentration of carbonate ions in the liquid phase by 52% from 4.91×10^{-4} to 7.58×10^{-4} mol kg^{-1} based on PhreeqC calculations, which contributed to the enhancement in the extent of olivine carbonation with increasing temperature. Our studies indicated that as olivine was dissolved, the presence of carbonate ions served as a sink for Mg by forming magnesium carbonate. As a result, there was a constant driving force facilitating the release of Mg into solution, which was also favored by the decrease in the solubility of magnesite with increasing temperature.

Considering that the extent of olivine carbonation drastically increased from 3.0% at 90 °C to 85.3% at 185 °C, a large variation in the particle size and particle size distribution of the mineral slurry system was expected for products of reaction at different reaction temperatures. There are two competing factors influencing the particle size of the mineral particulate system: size reduction *via* mineral dissolution and size increase due to carbonate precipitation on remaining olivine particles. Instead, it was found that the mean particle size before and after the carbonation reaction was not significantly changed. However, there was an interesting trend in the particle size and size distribution as a function of reaction temperature.

As shown in Fig. 4(a) and (b), at lower temperatures (90–125 °C), the measured mean particle sizes after olivine carbonation were slightly smaller (15.36–18.51 μm) than that of unreacted olivine (21.40 μm) whereas the Mg concentration was highest and the overall extent of carbonation remained low as discussed earlier. This suggests that olivine dissolution dominated over magnesium carbonate precipitation at the lower end of our experimental temperature range. On the other hand, at 150 and 185 °C, an increase in the mean particle size from 21.40 (unreacted) to 25.40 and 27.34 μm was observed. The narrower particle size distribution at higher reaction temperatures led to an increased mean particle size while the upper limit of the particle size was slightly reduced.

With an enhanced rate of mineral dissolution at high temperatures, a rapid disappearance of fines (<10 μm) was expected. Fig. 4(b) does show such a trend in all cases except there was an increased number of fines for the 90 °C case. A comparison of the SEM images in Fig. 5 along with the previously discussed solid and liquid sample analyses suggests that fines were mostly likely small silica particles detached from the incongruently dissolved olivine surface, or small, newly nucleated magnesite crystals. For the higher temperature cases, such as at 185 °C, significant magnesite growth to form larger crystals was evident.

BET analyses revealed that the surface area decreased from 3.77 (unreacted) to 2.01, 1.10, 1.07 and 0.96 $m^2\ g^{-1}$ at 90, 125, 150 and 185 °C, respectively, during olivine carbonation (Table 2). As shown in Fig. 4(c), the changes in the cumulative pore volume followed the same trend as the surface area. The cumulative pore volume decreased from 0.012 (unreacted) to 0.0087, 0.0033, 0.0027 and 0.0026 $m^2\ g^{-1}$ at 90, 125, 150 and 185 °C, respectively. At higher temperatures where greater extents of olivine carbonation were achieved, the decrease in the cumulative pore volume was more notable due to the formation of carbonates in the pore spaces.

XRD analyses were performed to identify the carbonated minerals, since the formation of different carbonate phases would influence the morphological characteristics of the carbonated mineral. Prior studies have reported that reaction temperature is an important factor in controlling precipitation of nesquehonite ($MgCO_3{\cdot}3H_2O$), hydromagnesite ($Mg_5(CO_3)_4(OH)_2{\cdot}4H_2O$) and magnesite ($MgCO_3$) in the order of increasing temperature.[18–20]

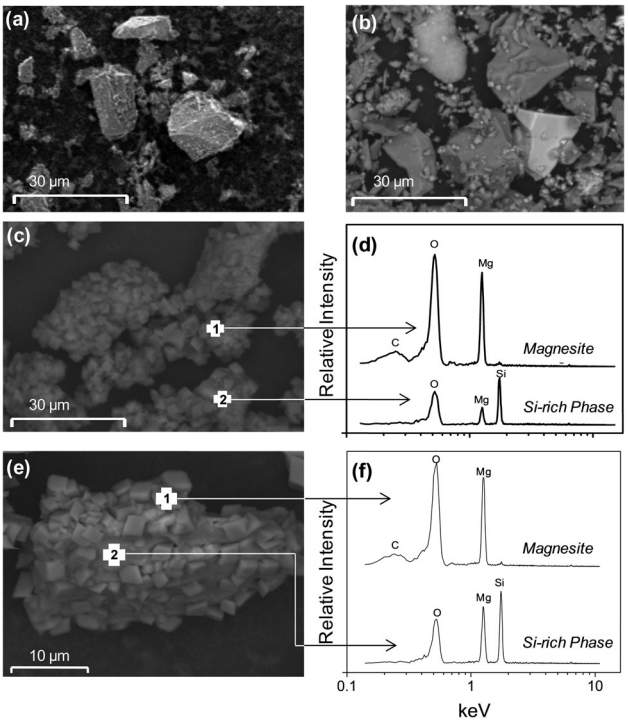

Fig. 5 Comparison of morphological changes of (a) unreacted olivine, (b) olivine reacted at 90 °C, (c) and (e) olivine reacted at 185 °C where (d) and (f) represent the identification of magnesite and silica-rich phases *via* EDS, respectively. Experiments were performed at P_{CO_2} = 139 atm in 1.0 M NaCl + 0.64 M $NaHCO_3$ for 3 hours with 15 wt% solid and a stirring rate of 800 rpm.

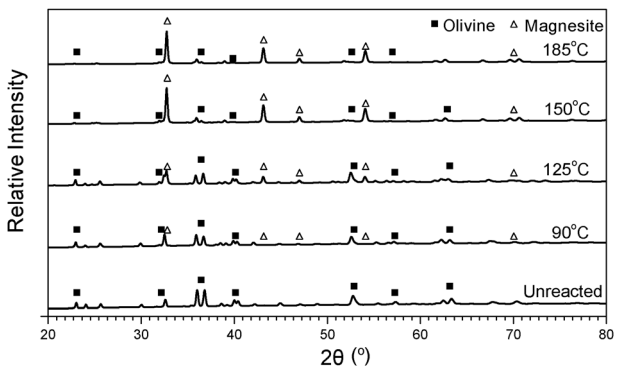

Fig. 6 Phase transformation of olivine *via* carbonation at different temperatures. XRD patterns for samples carbonated at P_{CO_2} = 139 atm, in 1.0 M NaCl + 0.64 M $NaHCO_3$ for 3 hours with 15 wt% solid and a stirring speed of 800 rpm.

With increasing temperature, the coordination of water molecules is disrupted which results in the formation of magnesite.[18] The XRD patterns of carbonated olivine samples in our study, shown in Fig. 6, revealed that magnesite was the dominant carbonate phase across the temperature range studied (90–185 °C), which agrees with the prior studies.[18] Thus, it was concluded that the morphological changes in carbonated olivine at different temperatures was not due to a change in the type of Mg-carbonate. Meanwhile, as shown in Fig. 5(b) and (c) the changes in the overall morphology of the carbonated olivine system, containing $MgCO_3$ as well as silica and unreacted olivine, were strongly affected by the extent of carbonation and the location of carbonation precipitation (*i.e.*, on or away from the olivine substrate). The formation of magnesite and silica rich phases as discussed in Béarat *et al.*,[37] King *et al.*,[38] and Daval *et al.*,[39] was evident from Fig. 5(c)–(f). The reduction in the pore spaces is attributed to the extensive growth of magnesite on the surface of olivine grains as evident from Fig. 5(e). Hövelmann *et al.* concluded that carbonation of only 10% reduced the porosity by half, and concluded that the carbonation reaction was self-limiting.[29] In our studies, however, despite almost an order of magnitude decrease in the pore volume of reacted olivine at 185 °C compared to unreacted olivine, about 85% carbonation was achieved. Since the highest carbonation of olivine was achieved at 185 °C, in this and previous studies, all subsequent experiments were performed at this temperature.

3.5. Role of $NaHCO_3$

Prior studies at ARC and Arizona State University revealed a significant enhancement in the rate of olivine carbonation in the presence of $NaHCO_3$. However, the prior experiments were all conducted in aqueous solutions including 1.0 M NaCl, so that the independent role of $NaHCO_3$ was not clearly quantified. Indeed, minor rate enhancements due to the presence of dissolved salts have been reported.[13,40,41] However, it is clear from studies of the olivine carbonation rate as a function of varying dissolved $NaHCO_3$, $KHCO_3$ and $RbHCO_3$ concentrations that most of the rate enhancement due to the dissolved species in these studies derives from dissolved bicarbonate.[28] The improved olivine carbonation rate was explained as a ''catalytic effect'' since the bicarbonate concentrations in the liquid phase did not significantly change before and after the carbonation experiments.[26–28] However, the actual bicarbonate concentration during the reaction at elevated temperature and P_{CO_2} was not reported, and thus, it has also been suggested that the role of $NaHCO_3$ may not be catalytic but rather buffering. Furthermore, by providing initial high concentration of bicarbonate ions, a potential rate-limiting CO_2 hydration step could be bypassed and the equilibrium can be shifted towards producing more carbonate ions to react with dissolved Mg ions. In order to isolate the effect of $NaHCO_3$ and investigate proposed mechanisms of rate enhancement, a series of experiments was performed at different $NaHCO_3$ concentrations while monitoring the extent of olivine carbonation as well as the corresponding chemical and morphological changes. The findings from this study were compared to results of 1 hour experiments performed by Chizmeshya *et al.* at Arizona State University (ASU).[28]

In this study, olivine carbonation experiments with varying concentrations of $NaHCO_3$ were performed for a reaction time of 3 hours, while keeping the reaction temperature of 185 °C and P_{CO_2} of 139 atm with 15 wt% solid and a stirring rate of 800 rpm. There was no dissolved NaCl in the fluid. Considering the formation of Mg and Ca-carbonates (*i.e.*, no siderite formation), the extents of olivine carbonation were reported as an average of TGA and TCA estimates. For deionized water containing 0.32, 0.48, 0.64, 1.0 and 2.0 M $NaHCO_3$, the extents of

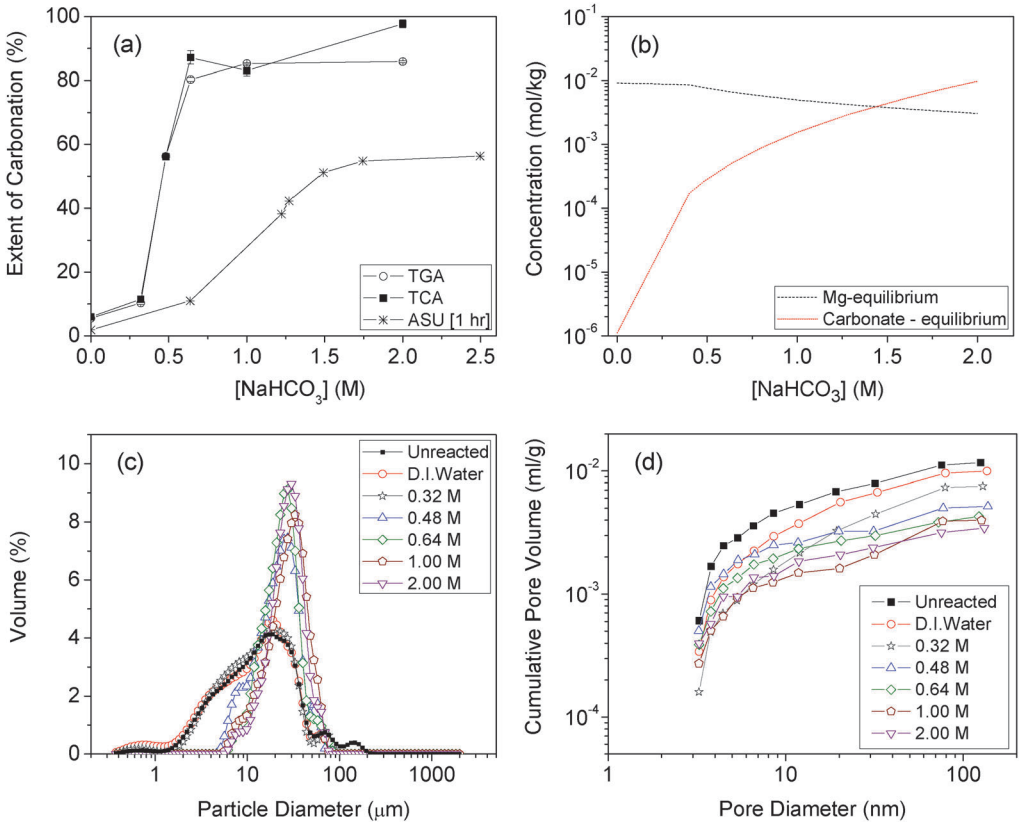

Fig. 7 Effect of $NaHCO_3$ concentration on (a) extent of olivine carbonation based on the formation of Mg and Ca carbonates, (b) simulated Mg and CO_3^{2-} concentrations, (c) particle size distribution, and (d) cumulative pore volume. Experiments were conducted at 185 °C, at P_{CO_2} = 139 atm, for 3 hours, with 15 wt% solid and a stirring speed of 800 rpm. ASU study was performed under same conditions but for 1 hour, P_{CO_2} = 150 atm, 1500 rpm, and included Fe-carbonate formation.[28]

olivine carbonation were found to be 5.8, 10.9, 56.0, 82.7, 85.0 and 91.2%, respectively (Table 2 and Fig. 7(a)). Addition of $NaHCO_3$ substantially increased the extent of olivine carbonation, though this effect was smaller at $NaHCO_3$ concentrations higher than 0.64 M. This trend matched that of the experiments performed at ASU[28] for a reaction time of 1 hour. The extents of olivine carbonation in ASU experiments, in the range of 1.5–2.5 M $NaHCO_3$, match the conversion results of this study performed for 1 hour in 1.0 M NaCl + 0.64 M $NaHCO_3$ shown in Fig. 2, implying that the difference between this study and the ASU study was mainly due to the reaction time difference.

It was also interesting to notice that while most TGA and TCA estimates were in close agreement, the extents of olivine carbonation in 2.0 M $NaHCO_3$ solvent estimated *via* TGA and TCA methods differed by about 11%, which confirmed the importance of selecting the suitable carbon analysis method for mineral carbonation studies. This only occurred at the highest $NaHCO_3$ concentration because while 2.0 M $NaHCO_3$ is soluble at 185 °C, the precipitation of $NaHCO_3$ may have occurred as the reactor was cooled before sampling. As a result, the TGA method, which can distinguish different carbon-containing phases, was probably more accurate than the TCA method. Decomposition of $NaHCO_3$ in the reacted sample was observed at 150 °C forming Na_2CO_3, CO_2 and H_2O, whereas the calcination of magnesite occurs at 560–680 °C.[42] Therefore, only the second weight drop in the TGA analysis was used to estimate the extent of olivine carbonation. On the other hand, a significantly higher extent of carbonation would be estimated *via* the TCA method since all carbon in the solid sample – potentially including precipitated $NaHCO_3$ – would be used for the calculation.

The non-linear behavior shown in Fig. 7(a) suggests that the role of $NaHCO_3$ on olivine carbonation is complex and multi-faceted. As discussed earlier, olivine dissolution and carbonate mineral precipitation are two key, sequential reactions determining the overall mineral carbonation rate. Depending on the reaction conditions (*e.g.*, pH, temperature, fluid composition), the rate-limiting step may differ. Fluid samples collected at the end of each run were analyzed using the ICP-AES. The Mg concentrations were 219.7, 74.5, 63.5, 55.1, 25.8 and 22.3 ppm in the reacted liquid samples for deionized water containing 0, 0.32, 0.48, 0.64, 1.0 and 2.0 M $NaHCO_3$, respectively. These Mg concentrations are consistently lower than the equilibrium values obtained from PhreeqC simulations that were 781, 223, 187, 158, 120 and 73.2 ppm in deionized water containing 0, 0.32, 0.48, 0.64, 1.0 and 2.0 M $NaHCO_3$, respectively. A direct comparison of these equilibrium concentrations with measured Mg concentrations cannot be made. While the equilibrium

concentrations can be calculated for the experimental conditions, the solution concentrations were measured at ambient conditions after the reactor was cooled, depressurized, and filtered to separate the reacted solid from the reaction fluid.

On the other hand, the trend of the extent of the olivine carbonation was affected by the relative concentrations of Mg and CO_3^{2-} in the liquid phase, which is a strong function of pH. The pH of each carbonation case simulated by PhreeqC showed an increase from 5.42 in deionized water to 6.37, 6.49, 6.69 and 7.05 in the presence of 0.48, 0.64, 1.0 and 2.0 M $NaHCO_3$, respectively. As shown in Fig. 7(b), over the pH range from 5.42 and 7.05, the equilibrium concentration of CO_3^{2-} changed significantly compared to that of Mg. This explains the small extent of olivine carbonation in the low $NaHCO_3$ case and the increased olivine carbonation at higher concentrations of $NaHCO_3$. As the CO_3^{2-} molar concentration approached and surpassed the Mg molar concentration at around 0.64–1 M $NaHCO_3$ (Fig. 7(b)), the extent of carbonation leveled off as the overall olivine carbonation became limited by the amount of dissolved Mg in the system (Fig. 7(a)). The comparison of the initial and final pHs of each CO_2–olivine–water system suggests that $NaHCO_3$ acted as a buffer to maintain relatively constant pH throughout the olivine carbonation process. For instance, in pure, deionized water the pH was changed from 7.00 to 5.42 during olivine carbonation, whereas it only changed from 7.78 to 7.05 when the same reactions were performed in 2.0 M $NaHCO_3$ solution.

Additional insights into the role of $NaHCO_3$ were provided *via* analyses of particle and pore size distributions. The particle size decreased slightly from 21.4 μm (unreacted) to 16.43 and 17.64 μm after carbonation reaction in deionized water with 0 and 0.32 M $NaHCO_3$, which indicates that mineral dissolution controlled the morphological changes of the remaining olivine particles. It is also interesting to note that olivine reacted in deionized water had a reddish-brown color indicating the precipitation of an iron oxide phase on the surface of olivine particles. (This was also observed in the case of NaCl only cases, described below.) On the other hand, no iron oxide precipitation was detected in all the experimental runs with more concentrated $NaHCO_3$ in solution, regardless of the presence or absence of NaCl. Olivine reacted with fluids containing $NaHCO_3$ concentrations of 0.48 M or higher had a mean particle size in the range of 26–30 μm, notably larger than that of unreacted olivine. As shown in Fig. 7(c), a progressively narrower particle size distribution, shifted toward larger particles, was observed with increasing $NaHCO_3$ concentration. As in other experiments described in previous sections of this paper, both the dissolution of fine particles with a large surface area to volume ratio, and the precipitation of new phases (mainly magnesite), reduced the overall surface area of carbonated olivine particles from 3.77 $m^2\ g^{-1}$ for unreacted olivine to 2.79, 1.63, 1.51, 1.20, 1.15 and 1.15 $m^2\ g^{-1}$ for olivine reacted in deionized water, 0.32, 0.48, 0.64, 1.0 and 2.0 M $NaHCO_3$, respectively.

A comparison of the cumulative pore volume of reacted olivine samples revealed similar trends as the changes in their surface area. The cumulative pore volume decreased from 0.012 ml g^{-1} for unreacted olivine to 0.01, 0.0075, 0.0052, 0.0043, 0.004 and 0.0035 ml g^{-1} for olivine reacted in deionized water with 0, 0.32, 0.48, 0.64, 1.0 and 2.0 M $NaHCO_3$, respectively. As illustrated earlier, higher extents of olivine carbonation resulted in a significant reduction in the cumulative pore volumes as magnesium carbonates precipitated in the pores. In the case of deionized water, the precipitation of iron oxide may have also contributed to a reduction in the pore volume.

A comparison of the extents of olivine carbonation in 1.0 M NaCl + 0.64 M $NaHCO_3$ with 0.64 M $NaHCO_3$ and 1.0 M $NaHCO_3$ alone revealed that the extents of carbonation were 85.3%, 82.7% and 85% respectively with a deviation of about ±2–4%. Therefore, the effect of 1.0 M NaCl on enhancing carbonation did not appear to be significant. In order to delineate the role of NaCl further, olivine carbonation experiments with varying concentrations of NaCl were performed as discussed in the following section.

3.6. Role of NaCl

In order to further isolate the effects of $NaHCO_3$ and NaCl on olivine carbonation, a series of experiments were performed at different NaCl concentrations ranging from 0.5 to 1 M in the absence of $NaHCO_3$, with other reaction parameters the same as for the experiments described in Section 3.5. A better understanding of the role of NaCl will provide insight into how saline water in deep, subsurface aquifers may impact olivine carbonation. Some have reported that compared to geologically slow natural weathering of olivine, Cl^- slightly enhances the magnesium silicate dissolution rate by forming a weak bond with MgO, and thereby disrupting the crystal structure of the mineral and facilitating mineral dissolution[27] while other studies revealed that varying the salt concentration changes the pH which in turn affects the dissolution behavior of olivine.[40] The role of cations such as K^+ or Na^+ is not as well understood, although it has been suggested that these cations may facilitate ion exchange across the solid/liquid interface by altering the surface charges.[27]

As shown in Fig. 8(a), the extents of olivine carbonation in fluids containing only NaCl were low compared to all other experimental cases. Even at the highest concentration of 1.0 M NaCl, olivine carbonation was limited to 14.1% in three hours, about twice the 6.0% extent of carbonation in deionized water. Thus, in the absence of a buffer such as $NaHCO_3$, olivine carbonation involving saline fluids would not be sufficiently fast to achieve a high degree of olivine carbonation within a few hours. PhreeqC calculations suggest that in the presence of 139 atm CO_2 pressure, the pH of 1.0 M NaCl solution would be 5.51, whereas the calculated pH of 0.64 M $NaHCO_3$ and 1.0 M NaCl + 0.64 M $NaHCO_3$ solutions were 6.31 and 6.36, respectively. With lowered reaction pH, the concentrations of Mg in liquid samples were estimated to be greater than those in systems with higher, buffered pH (*i.e.*, 219.7, 148.4, 123.2 and 95.7 ppm in deionized water, with 0, 0.5 M, 0.75 M and 1.0 M NaCl, respectively). The lower pH in 1.0 M NaCl solvent may have inhibited the formation of solid carbonate phases.

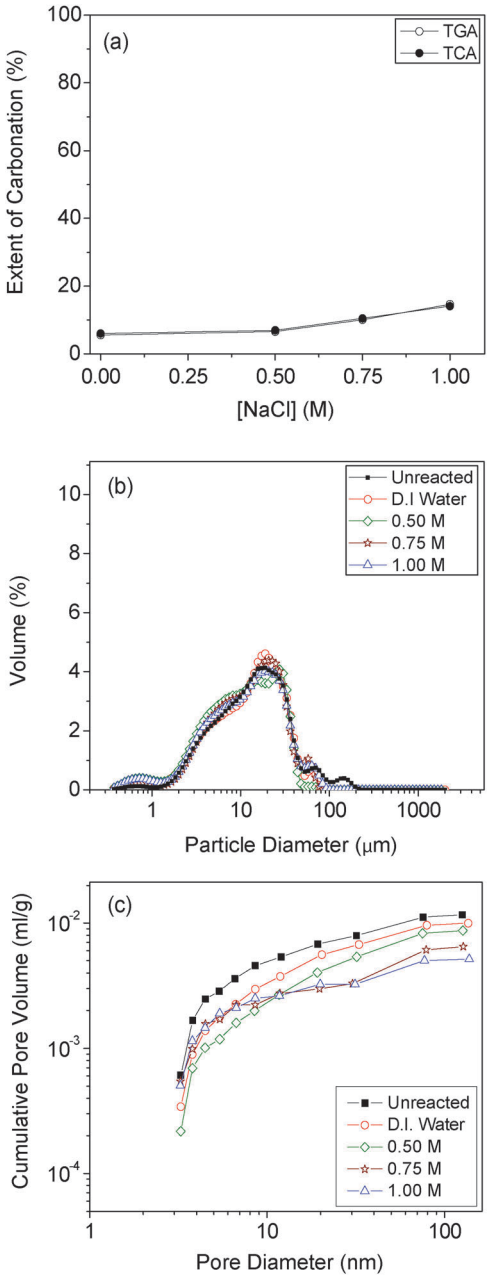

Fig. 8 Effect of NaCl concentration on (a) extent of olivine carbonation based on the formation of Mg and Ca carbonates, (b) particle size distribution, and (c) cumulative pore volume. Experiments were conducted at 185 °C, at P_{CO_2} = 139 atm, for 3 hours, with 15 wt% solid and a stirring speed of 800 rpm.

Increasing the concentration of NaCl has also been reported to increase the ionic strength and in turn decrease the solubility of CO_2.[43] Studies by King *et al.*, revealed that increasing the ionic strength reduced the activity of water and aided the precipitation of magnesite.[38]

In the presence of NaCl, without $NaHCO_3$, the particle size distribution remained almost unchanged (Fig. 8(b)). As NaCl concentration increased from 0.5 to 1.0 M, the mean particle size, surface area and cumulative pore volume were slightly decreased (see Table 2 and Fig. 8(c)). While the changes in the morphological characteristics of olivine during its carbonation in the presence of NaCl were minimal, all olivine samples carbonated in the presence of $NaHCO_3$ showed lighter and whiter colors, but olivine carbonated without $NaHCO_3$ was distinctively reddish brown due to precipitation of iron oxides on olivine surfaces. The formation of this amorphous iron oxide layer, and its role in inhibiting mineral dissolution, have been previously reported.[23,27,33] Other studies reported the precipitation of hematite at shorter reaction times but not at longer durations due to changes in the fluid composition, and carbonate concentrations over time.[38] In the absence of a pH buffer (*i.e.*, $NaHCO_3$), the olivine–NaCl solution–CO_2 system may experience an internal pH swing, which could have led to the precipitation of iron oxides.

4. Conclusions

Olivine, an abundant, reactive silicate mineral suitable for mineral carbonation processes, was evaluated for its CO_2 storage capacity. Direct olivine carbonation is a complicated phenomenon due to simultaneous chemical and morphological changes in the olivine grains. For both *in situ* and *ex situ* carbon storage schemes *via* mineral carbonation, it is important to understand the reaction mechanisms and kinetics in order to estimate the CO_2 uptake rate, storage capacity, and long term stability of the geologically stored CO_2. This study showed that the reaction time, temperature, CO_2 pressure and fluid composition all have first-order effects on carbonation rates and reaction mechanisms. Olivine carbonation is considerably enhanced in solutions containing $NaHCO_3$, with or without dissolved NaCl. We infer that $NaHCO_3$ is not a catalyst, but rather serves as a pH buffer and a source of carbonate ions. At high $NaHCO_3$ concentrations, the calculated system pH was high (>6.5) and thus, carbonate ions were more readily available for the formation of magnesium carbonate. In turn this lowers the Mg concentration in the fluid, which drives ongoing olivine dissolution. NaCl alone does not significantly enhance olivine carbonation. In some experiments using deionized water, with and without dissolved, NaCl, iron oxide precipitation was observed. Iron oxides did not precipitate in experiments with more than 0.32 M $NaHCO_3$. Overall, the results of this study are consistent with studies performed at Albany Research Center and Arizona State University.[26–28]

In addition to changes in the chemical compositions of the solid and liquid phases, detailed analyses of the particle and pore size distributions revealed that as olivine dissolved, pores surrounded by Si-rich phases were opened, and magnesium carbonate phases precipitated in these pores, thereby limiting the pore space available for further reactivity. The changes in the pore volume may impact the long-term CO_2 storage capacity and need to be taken into account in future modeling studies to predict the long-term fate of CO_2. Order of magnitude estimates of the olivine carbonation rate – in mass fraction of olivine carbonated, per second – in the presence of aqueous fluids with more than ~0.5 M $NaHCO_3$, with grain sizes of tens of

microns, can be confidently calculated using the expression developed by Kelemen and Matter[1] for the ARC results,[27] which is very similar to the expression derived based on the data presented in this study. While the expression derived in Kelemen and Matter,[1] provided a somewhat better fit to the ARC[27] data alone, the second one (eqn (13)) may be more robust in some ways. Alternatively, different results from the two expressions can be interpreted as a partial indication of the current level of uncertainty in olivine carbonation rates under the relevant experimental conditions.

Nomenclature

M	Alkaline metal
W_{CO_2}	Weight of CO_2
$W_{mineral}$	Weight of mineral
R_{CO_2}	Mass of raw mineral needed to store a unit mass of CO_2
$1/R_{CO_2}$	Mass of CO_2 stored in a unit mass of mineral
y_m	Weight fraction of alkaline metal in mineral that can react with CO_2 to form carbonates
MW_m	Molecular weight of alkaline metal, M
MW_{CO_2}	Molecular weight of CO_2 (44 g mol^{-1})
$Y_{CO_2,TGA}$	Yield or extent of carbonation: mass of CO_2 stored in the mineral as solid carbonate measured *via* TGA, relative to CO_2 storage capacity
TGA	The percent weight change of the solid sample at its calcination temperature $\left(=\left[\frac{\text{Weight of } CO_2 \text{ released}}{\text{Weight of solid sample}}\right]\times 100\%\right)$
$Y_{CO_2,TCA}$	Yield or extent of carbonation: mass of CO_2 stored in the mineral as solid carbonate measured *via* TCA, relative to the CO_2 storage capacity
TCA	The weight fraction of carbon in the solid sample $\left(=\left[\frac{\text{Weight of carbon}}{\text{Weight of solid sample}}\right]\right)$
P_{CO_2}	Partial pressure of CO_2 (atm)

Acknowledgements

This publication was based on work supported by the U.S. Department of Energy (DE-FE0002386). Kelemen was also supported in part by NSF Research Grant EAR 1049905.

References

1 P. B. Kelemen and J. Matter, *Proc. Natl. Acad. Sci. U. S. A.*, 2008, **105**, 17295–17300.
2 J. M. Matter and P. B. Kelemen, *Nat. Geosci.*, 2009, **2**, 837–841.
3 P. B. Kelemen, J. Matter, E. E. Streit, J. F. Rudge, W. B. Curry and J. Blusztajn, *Annu. Rev. Earth Planet. Sci.*, 2011, **39**, 545–576.
4 P. B. Kelemen and G. Hirth, *Earth Planet. Sci. Lett.*, 2012, **345–348**, 81–89.
5 A. Nicolas, E. Boudier, B. Ildefonse and E. Ball, *Mar. Geophys. Res.*, 2000, **21**, 147–179.
6 W. Seifritz, *Nature*, 1990, **345**, 486.
7 K. S. Lackner, *Annu. Rev. Energy Environ.*, 2002, **27**, 193–232.
8 X. Wang, W. Conway, R. Burns, N. McCann and M. Maeder, *J. Phys. Chem. A*, 2010, **114**, 1734–1740.
9 A. Stirling and I. Papai, *J. Phys. Chem. B*, 2010, **114**, 16854–16859.
10 A. Awad, A. F. K. van Groos and S. Guggenheim, *Geochim. Cosmochim. Acta*, 2000, **64**, 1765–1772.
11 Y. Chen and S. L. Brantley, *Chem. Geol.*, 2000, **165**, 267–281.
12 D. E. Giammar, R. G. Bruant Jr. and C. A. Peters, *Chem. Geol.*, 2005, **217**, 257–276.
13 M. Hanchen, V. Prigiobbe, G. Storti, T. M. Seward and M. Mazzoti, *Geochim. Cosmochim. Acta*, 2006, **70**, 4403–4416.
14 E. H. Oelkers, *Chem. Geol.*, 2001, **175**, 485–494.
15 O. S. Pokrovsky and J. Schott, *Geochim. Cosmochim. Acta*, 2000, **64**, 3313–3325.
16 P. V. Brady, R. I. Dorn, A. J. Brazel, J. Clark, R. B. Moore and T. Glidewell, *Geochim. Cosmochim. Acta*, 1999, **63**, 3293–3300.
17 R. A. Wogelius and J. V. Walther, *Chem. Geol.*, 1992, **97**, 101–112.
18 M. Hanchen, V. Prigiobbe, R. Baciocchi and M. Mazzotti, *Chem. Eng. Sci.*, 2008, **63**, 1012–1028.
19 G. D. Saldi, G. Jordan, J. Schott and E. H. Oelkers, *Geochim. Cosmochim. Acta*, 2009, **73**, 5646–5657.
20 G. D. Saldi, J. Schott, O. S. Pokrovsky and E. H. Oelkers, *Geochim. Cosmochim. Acta*, 2012, **83**, 93–109.
21 S. R. Gislason, D. Wolff-Boenisch, A. Stefansson, E. H. Oelkers, E. Gunnlaugsson, H. Sigurdardottir, B. Sigfusson, W. S. Broecker, J. M. Matter, M. Stute, G. Axelsson and T. Fridriksson, *Int. J. Greenhouse Gas Control*, 2010, **4**, 537–545.
22 B. P. McGrail, H. T. Schaef, A. M. Ho, Y. J. Chien, J. J. Dooley and C. L. Davidson, *J. Geophys. Res.*, 2006, **111**, 1–13.
23 A.-H. A. Park, R. Jadhav and L.-S. Fan, *Can. J. Chem. Eng.*, 2003, **81**, 885–890.
24 A.-H. A. Park and L.-S. Fan, *Chem. Eng. Sci.*, 2004, **59**, 5241–5247.
25 T. M. Yegulalp, K. S. Lackner and H. J. Ziock, *Int. J. Surf. Min., Reclam. Environ.*, 2001, **15**, 52–68.
26 S. J. Gerdemann, W. K. O'Connor, D. C. Dahlin, L. R. Penner and H. Rush, *Environ. Sci. Technol.*, 2007, **41**, 2587–2593.
27 W. K. O'Connor, D. C. Dahlin, G. E. Rush, S. J. Gerdemann, D. N. Nilsen, *Final report: aqueous mineral carbonation*, 2004, DOE/ARC-TR-04-002.
28 A. V. G. Chizmeshya, M. J. McKelvy, K. Squires, R. W. Carpenter and H. Bearat, DOE Final Report 924162: A novel approach to mineral carbonation: enhancing carbonation while avoiding mineral pretreatment process cost, 2007.
29 J. Hövelmann, H. Austrheim and B. Jamtveit, *Chem. Geol.*, 2012, **334**, 254–265.
30 T. Xu, J. A. Apps and K. Pruess, *Appl. Geochem.*, 2004, **19**, 917–936.
31 J. G. Watson, J. C. Chow and L.-W. A. Chen, *Aerosol Air Qual. Res.*, 2005, **5**, 65–102.
32 F. Demir, B. Donmez, H. Okur and F. Sevim, *Chem. Eng. Res. Des.*, 2003, **81**, 618–622.

33 G. D. Saldi, D. Daval, G. Morvan and K. G. Knauss, *Geochim. Cosmochim. Acta*, 2013, **118**, 157–183.
34 D. L. Parkhust and C. A. J. Appelo, User's guide to PHREEQC (Version 2). Water Resources Investigations Report 99–4259. U.S. Geological Survey, Denver, CO, 1999.
35 P. Benezeth, G. D. Saldi, J.-L. Dandurand and J. Schott, *Chem. Geol.*, 2011, **286**, 21–31.
36 J. L. Palandri and Y. K. Kharaka, *U.S. Geol. Surv. Open File Rep*. 2004-1068, U.S. Geol. Surv., Menlo Park, CA, 2004.
37 H. Béarat, M. J. McKelvy, A. V. G. Chizmeshya, D. Gormley, R. Nunez, R. W. Carpenter, K. Squires and G. H. Wolf, *Environ. Sci. Technol.*, 2006, **40**, 4802–4808.
38 H. E. King, O. Plümper and A. Putnis, *Environ. Sci. Technol.*, 2010, **44**, 6503–6509.
39 D. Daval, O. Sissmann, N. Menguy, G. D. Saldi, F. Guyot, I. Martinez, J. Corvisier, B. Garcia, I. Machouk, K. G. Knauss and R. Hellmann, *Chem. Geol.*, 2011, **284**, 193–209.
40 A. A. Olsen, *Forsterite dissolution kinetics: applications and implications for chemical weathering*, PhD thesis, Virginia Polytechnic Institute, Blacksburg, VA, USA, 2007.
41 V. Prigiobbe, G. Costa, R. Baciocchi, M. Hänchen and M. Mazzotti, *Chem. Eng. Sci.*, 2009, **64**, 3510–3515.
42 P. K. Heda, D. Dollimore, K. S. Alexander, D. Chen, E. Law and P. Bicknell, *Thermochim. Acta*, 1995, **255**, 255–272.
43 Z. Duan, R. Sun, C. Zhu and I. Chou, *Mar. Chem.*, 2006, **98**, 131–139.